PAPER

CrossMark
← click for updates

Down- and up-converting dual-mode YPO$_4$:Yb^{3+}, Tb^{3+} nanocrystals: synthesis and spectroscopic properties†

Tomasz Grzyb,*[a] Rafal J. Wiglusz,[b] Aleksandra Gruszeczka[a] and Stefan Lis[a]

Tetragonal YPO$_4$ nanocrystals doped with Yb^{3+} and Tb^{3+} ions were synthesized by 900 °C annealing of precursors obtained with a co-precipitation method in the presence of glycerine. These materials exhibited intense green luminescence under ultraviolet excitation and up-conversion emission from the $^5D_3$ and $^5D_4$ Tb^{3+} excited states after irradiation with near infrared light (λ = 980 nm). The structure and morphology of the products were analysed by recording X-ray diffraction patterns and transmission electron microscopy images. The obtained nanomaterials were single-phased with spherical shaped nanocrystals that had an average size of 18 ± 3 nm. The spectroscopic properties of YPO$_4$:Yb^{3+},Tb^{3+} nanocrystals were investigated based on their excitation and emission spectra. The time-resolved luminescence traces were measured, and the luminescence lifetimes of Tb^{3+} and Yb^{3+} ions were calculated. The most effective dopant concentrations were determined to be 5% Yb^{3+} and 15% Tb^{3+}, which exhibited the most intense ultraviolet excited emission and up-conversion. Because the integral intensity was observed to be dependent on the power of the pumping laser, a cooperative energy transfer (CET) mechanism underlying the observed up-conversion was proposed.

Introduction

In recent decades, efforts to synthesize new luminescent nanomaterials activated by lanthanide (Ln^{3+}) ions have been the subject of intense research.[1–5] Luminescent Ln^{3+}-doped materials are required for next generation plasma display panels (PDPs), mercury-free fluorescence lamps, fiber amplifiers, forensic sciences and particularly light emitting diodes (LEDs).[6–9] However, materials that exhibit up-conversion (UC) properties have attracted special attention due to their potential applications in solving current challenges in cancer diagnosis and therapy as well as in the utilization of solar energy. Therefore, there is growing interest in developing up-conversion nanocrystals for various applications, such as bioimaging, photodynamic therapy and drug delivery.[10–14] UC in solar cells has been developed to improve spectral absorption properties of the materials and their efficiencies.[15,16]

Rare earth (RE^{3+}) orthophosphates have been extensively investigated because they are promising hosts for emitting

Ln^{3+} ions.[17,18] Their very low solubility in water, high thermal stability and high quantum efficiencies for REPO$_4$-based phosphors are advantageous for the above mentioned applications.[19] Up-conversion orthophosphates in the form of nanocrystals have been studied since 2003.[20]

Lanthanide phosphates occur in two crystal structure forms including xenotime with a tetragonal structure and monazite with a monoclinic structure.[21] The xenotime structure is preferred by the heavy lanthanide ions from Tb^{3+} to Lu^{3+} with REO$_8$ polyhedron structures. However, the monazite structure is typically observed for the light lanthanides (from La^{3+} to Gd^{3+} ions) and larger REO$_9$ polyhedra.[21]

Up-conversion is a process in which two or more photons from the infrared or near infrared (NIR) range can be converted to photons with a higher energy than the absorbed energy (*i.e.* typically from the visible or ultraviolet spectral range). The idea of sequential absorption was proposed by Bloembergen in 1959.[22] However, the energy transfer process, which is important for Ln^{3+}-doped materials, leading to up-conversion emission was reported by Auzel in 1966.[23,24] Since that time, numerous studies have been performed.[1,2,25–29] In addition, the mechanisms of up-conversion have been studied, and the main mechanisms responsible for the anti-Stokes emission in Ln^{3+}-doped systems (*i.e.* ground/excited state absorption (GSA and ESA), energy transfer up-conversion (ETU), photon avalanche (PA) and cooperative energy transfer

[a]*Adam Mickiewicz University, Faculty of Chemistry, Department of Rare Earths, Umultowska 89b, 61-614 Poznan, Poland. E-mail: tgrzyb@amu.edu.pl*
[b]*Institute of Low Temperature and Structure Research, Polish Academy of Sciences, P.O. Box 1410, 50-950 Wroclaw, Poland*
†Electronic supplementary information (ESI) available: Luminescence decays of the YPO$_4$:Tb^{3+},Yb^{3+} nanocrystals. See DOI: 10.1039/c4dt02234c

(CET)) are known.[25] However, improvement in the efficiency of UC materials is still needed. In addition, the mechanisms of up-conversion in nanocrystalline systems consisting of Yb^{3+}–Tb^{3+} ions are still not well understood.

The up-conversion Yb^{3+}/Tb^{3+} pair of ions has been studied in many micro-materials, such as oxides, fluorides, glasses and polymers.[30–41] In addition, the luminescence of the Yb^{3+}/Tb^{3+} co-doped phosphates has been widely studied in relation to the cooperative energy transfer from two Tb^{3+} ions to one Yb^{3+} ion as a quantum cutting system by down-conversion.[42–44] However, investigations of down- and up-conversion in co-doped phosphates, especially in the nanocrystalline form, have been limited.[45–49] The Tb^{3+} ion exhibits high quantum efficiencies for luminescence due to the large energy gap between the ^7F_J ground state and the $^5D_4$ excited state, which results in the lack of multiphonon relaxation of the $^5D_4$ excited state and the high usage of this ion as a dopant in efficient phosphors. In addition, Yb^{3+} ions have many advantages as dopants resulting in their wide application as effective sensitizers for NIR radiation. One of the most important advantages is the high oscillator strength of the Yb^{3+} $^2F_{7/2} \rightarrow {}^2F_{5/2}$ transition responsible for the absorption of this ion at approximately 980 nm.

The main goal of the current paper is the evaluation of the physico-chemical properties of YPO_4 nanoparticles activated with Tb^{3+} and Yb^{3+} ions, with special emphasis on the luminescence properties of the obtained system. The role of the reaction conditions and the influence of the dopant concentration on the final form of the YPO_4 particles have been elucidated. The emission properties of the Yb^{3+} and Tb^{3+} co-doped system were fully characterized.

Experimental

Materials

All of the reagents were of analytical quality or spectral purity for rare earth oxides. To synthesize the materials, the following reagents were used: Y_2O_3, Yb_2O_3 and Tb_4O_7 were obtained from Stanford Materials (United States, 99.999%), nitric acid (HNO_3) was obtained from POCh S.A. (Poland, ultra-pure), ammonium phosphate monobasic ((NH_4)H_2PO_4) was obtained from Sigma-Aldrich (Poland, ReagentPlus®, ≥98.5%) and glycerine was obtained from POCh S.A. (Poland, pure p.a., 99.9%). Rare earth oxides were dissolved in HNO_3 to obtain their nitrates. 1 M solutions were used for further synthesis.

Synthesis of YPO_4:Yb^{3+},Tb^{3+} nanocrystals

Yttrium phosphate nanocrystals doped with Yb^{3+} and Tb^{3+} ions were prepared using a two-step method. First, the co-precipitation method was used to synthesize phosphates, which were thermally treated at 900 °C. The procedure for obtaining nanocrystals in the first stage is described below. 4 mmol of precipitate was formed in the reaction that was carried out in a beaker containing a 25% solution of glycerine in distilled water. To a beaker containing 100 mL of a glycerine

solution, 125% of the stoichiometric amount of $NH_4H_2PO_4$ was added. Next, the solution was magnetically stirred and heated to 50 °C. Simultaneously, 50 mL of the mixed solution containing $Y(NO_3)_3$, $Yb(NO_3)_3$ and $Tb(NO_3)_3$ was prepared by dissolving calculated volumes of rare earth nitrates in water at a concentration of 1 M, in a 25% solution of glycerine. The following concentrations of dopants ions were chosen: (i) the static molar concentration of Yb^{3+} was 10% and 5–30% of Tb^{3+} ions and (ii) the static molar concentration of Tb^{3+} ions was 15% and varied for Yb^{3+} ions in the range of 2.5–20% mol. After reaching the required temperature, the solution of RE^{3+} nitrates was poured into a dropping funnel and slowly added to the $NH_4H_2PO_4$ solution under magnetic stirring. The reaction was maintained for 30 min at approximately 50 °C. The white precipitate was centrifuged and washed several times with water and ethanol. The as-prepared powders were dried for 24 h at 80 °C in the air and annealed at 900 °C for 2 hours.

Characteristics of the YPO_4:Yb^{3+},Tb^{3+} nanocrystals

Powder diffractograms were recorded on a Bruker AXS D8 Advance diffractometer in Bragg–Brentano geometry with Cu $K_{\alpha 1}$ radiation in the 2θ range of 6° to 60°. The reference data were obtained from the Inorganic Crystal Structure Database (ICSD). In addition, X-ray diffractograms (XRD) were used in crystallographic data refinement along with the Rietveld method.[50,51] Transmission electron microscopy (TEM) images were recorded on a FEI Tecnai G2 20 X-TWIN transmission electron microscope with an accelerating voltage of 200 kV. High-resolution transmission electron microscopy (HRTEM) and selected area electron diffraction (SAED) images were recorded on a Philips CM-20 Super Twin electron microscope with an accelerating voltage of 200 kV.

A Hitachi F-7000 fluorescence spectrophotometer with a 150 W xenon lamp was used for determination of the luminescence properties (excitation and emission) of the samples at room temperature. The excitation and emission spectra were corrected for the instrumental response. For the up-conversion measurements, the solid state 980 nm laser (Dragon Lasers) was used as the excitation source. Emission lifetimes were measured at 545 nm (under excitation at the 978 nm line of a Ti:sapphire laser, LOTIS TII Belarus) using a Jobin-Yvon THR 1000 spectrophotometer (1200 mm^{-1} holographic grating), a Hamamatsu R928 photomultiplier as a detector and a digital oscilloscope LeCroy WaveSurfer 400 for data collection and on a QuantaMasterTM 40 spectrophotometer equipped with an Opolette 355LD UVDM tunable laser, which had a repetition rate of 20 Hz, as the excitation source and a Hamamatsu R928 photomultiplier as a detector. The decay curve fitting was performed using a single and double decay model with the Origin 9.0 software. The goodness of fit of the time traces was not less than $R^2 = 0.998$. Error bars presented in Fig. 10 and 11 were estimated by three times calculation of lifetime values from the experimental data and further statistical analysis.

Results and discussion

The methods for the synthesis of rare earth orthophosphates have been studied for many years due to interest in their structural properties.[52–54] Further studies have been performed to synthesize efficient $REPO_4$-based phosphors and investigate properties of Ln^{3+} luminescent ions incorporated into the $REPO_4$ structure as host materials.[17,18,42,55,56] Recently, many studies of $REPO_4$ synthesized nanomaterials have been reported.[45,47,57–59] Most of the developed methods of synthesis of $REPO_4$ powders or nanomaterials are based on the precipitation reaction between the RE^{3+} and PO_4^{3-} ions.

The co-precipitation method is one of the most widely used methods for nanomaterial synthesis.[60–62] This method is based on a chemical exchange reaction resulting in the precipitation of an insoluble inorganic compound. The major advantages of this method are that it is easy and inexpensive. However, some requirements must be met to synthesize nanocrystals with low aggregation, small particle sizes and narrow distributions. In addition, the reaction environment, which typically includes water, can result in a large amount of water being adsorbed on the nanocrystal surface. Therefore, in our reactions, glycerine has been used to inhibit excessive growth of nanoparticles and lower their aggregation.[3]

Structure and morphology

After the formation of $YPO_4:Yb^{3+},Tb^{3+}$, the XRD measurements were performed. All of the Bragg reflections in the diffraction patterns were indexed and assigned to the tetragonal crystal system $I4_1/amd$ space group no. 141 of the YPO_4 crystalline phases (see Fig. 1). No additional secondary phase, impurities or amorphous forms were observed, which confirmed the structural purity of the obtained compounds. This result confirmed that high lanthanide doping levels are achievable in
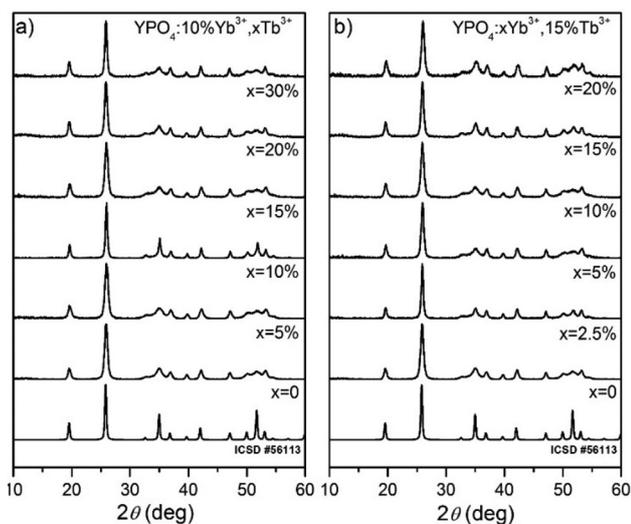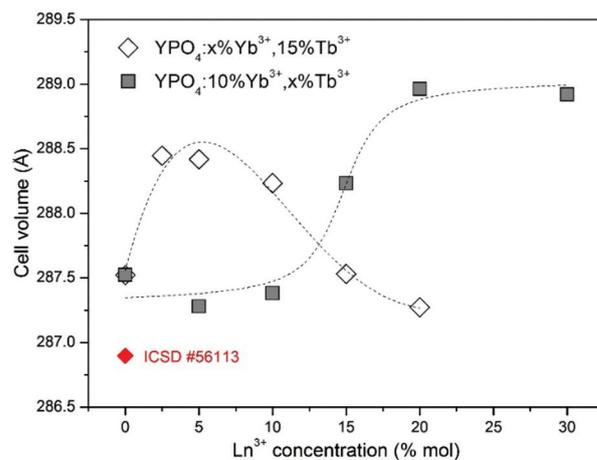

Fig. 2 Dependence of the crystal cell volumes of the $YPO_4:Yb^{3+},Tb^{3+}$ nanocrystals on the dopant ion concentration.

the YPO_4 host material without altering the structure of the host under the given synthesis conditions.

To determine the structural changes and calculate the cell parameters of the synthesized YPO_4 co-doped with Yb^{3+} and Tb^{3+} ions, Rietveld analysis has been used.[51] The structural refinement method has several advantages over conventional quantitative analysis methods. This method uses a whole pattern-fitting algorithm, and all of the lines are explicitly considered. Therefore, even severely overlapped lines are typically not a problem. The Rietveld refinement was performed based on YPO_4 crystals with a tetragonal structure using the crystallographic information file (CIF) no. 56113. Fig. 2 shows a comparison of the calculated cell volumes with the reference data. The crystallographic data and structural refinement indicated some changes in the structural parameters with the dopant concentrations.

The calculated cell volumes increased as the concentration of Tb^{3+} ions increased. For the Yb^{3+} doping, there was a decrease in the cell volumes as the concentration of this ion increased.

The significant difference between the unit cell parameters of the YPO_4 single crystal and those of the YPO_4 nanoparticles without dopant ions, which possess larger unit cell parameter values, is caused by the so-called grain size effect.[63,64]

In this phenomenon, a reduction in the particle size contributes to the creation of negative pressure on the crystal lattice, which causes expansion of the lattice cell volume. In the YPO_4 nanocrystals that are co-doped with Yb^{3+} and Tb^{3+}, two effects play a role in causing differences in the cell volumes between the reference and synthesized materials. The first effect is due to the above mentioned grain size effect. The second effect is related to the differences in the ionic radii of the Y^{3+}, Yb^{3+} and Tb^{3+} ions (for the coordination number, CN = 8, $r(Y^{3+})$ = 1.019 Å, $r(Tb^{3+})$ = 1.040 Å, $r(Yb^{3+})$ = 0.985 Å). Substitution of the Y^{3+} ions in the crystallographic structure by the smaller Yb^{3+} and bigger Tb^{3+} ions could result in contraction or expansion of the dimensions of the crystal cell.
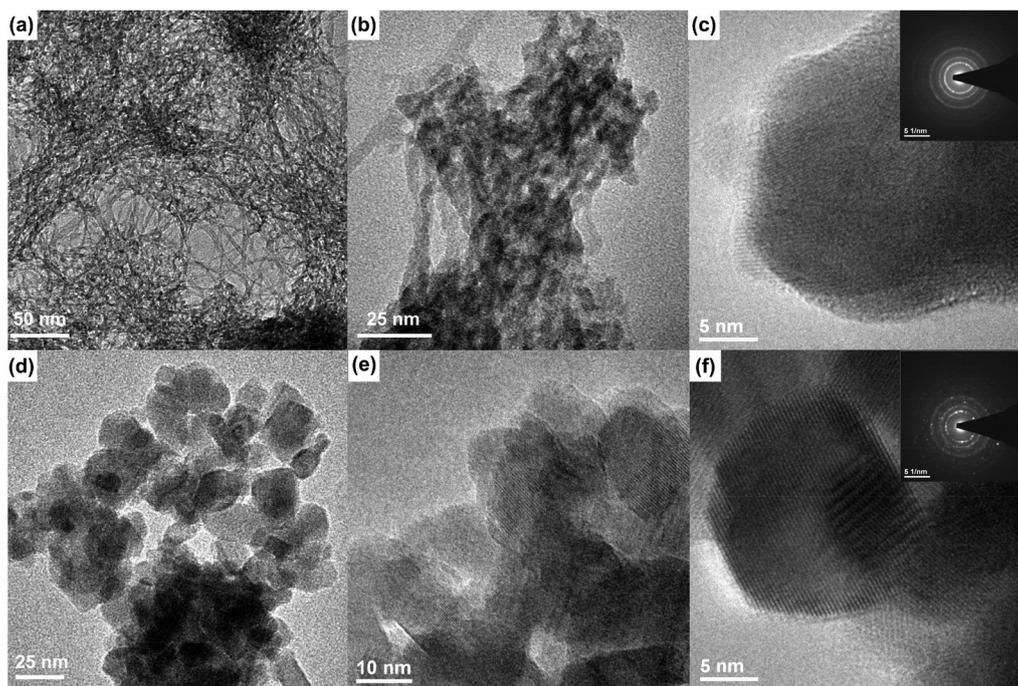

Fig. 1 XRD diffraction patterns of (a) 10% Yb^{3+}, x% Tb^{3+} doped YPO_4 and (b) x% Yb^{3+}, 15% Tb^{3+} doped YPO_4 nanocrystals annealed at 900 °C for 2 h.

Fig. 3 TEM and SAED images of the as-prepared (a–c) and annealed (d–f) YPO_4:5%Yb^{3+},15%Tb^{3+} nanocrystals (annealed at 900 °C for 2 hours).

The TEM images (see Fig. 3a) of the as-prepared sample indicate that after the co-precipitation reaction, nanofibers with a thickness of less than 5 nm are formed. Their length is difficult to estimate due to the web that is formed. The sample sintered at 900 °C for 2 h, which is shown in Fig. 3d–f, has considerably different morphology with nanocrystals that are rounded with an average size of 18 ± 3 nm. These crystal sizes are typical for powders prepared by the co-precipitation method and annealed at a higher temperature. High temperate also causes aggregation of crystallites.

Spectroscopic properties

The luminescence of the YPO_4:Yb^{3+},Tb^{3+} nanomaterials exhibits a dual nature. These nanomaterials can be excited by ultraviolet (UV) radiation due to the f–d and f–f electronic transitions within the Tb^{3+} ions or by NIR radiation due to Yb^{3+} absorption and energy transfer between dopants ions. Both excitation methods yield efficient green luminescence of the Tb^{3+} ions. The presence of Yb^{3+} and Tb^{3+} dopant ions has a strong influence on the observed luminescence properties because these ions are responsible for dual mode excitation and they can exchange energy, transfer charge and undergo other processes due to their complex spectroscopic nature and interactions between the ions. The luminescence excitation spectra were measured in the range of 200–400 nm and are shown in Fig. 4. These spectra are characterized by broad excitation peaks located at higher energies and a series of narrower peaks at lower energies. The broad excitation bands at shorter wavelengths (with maxima at approximately 225 nm in each sample) are associated with the $4f^8 \rightarrow 4f^7 5d^1$ transition in the Tb^{3+} ions, and the peaks located above 250 nm
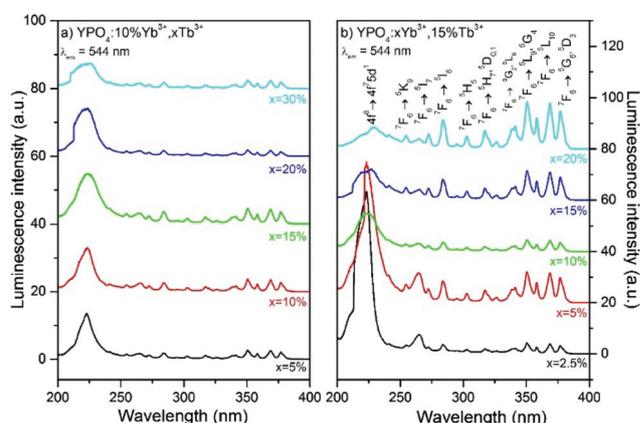

Fig. 4 Excitation spectra of (a) YPO_4 doped by 10% Yb^{3+}, x% Tb^{3+} and (b) YPO_4 doped by x% Yb^{3+}, 15% Tb^{3+}.

originated from the f–f electronic transitions characteristic of Tb^{3+} containing materials. By applying excitation with sufficiently energetic photons, electrons from the 4f electronic levels of Tb^{3+} ions can be promoted to the excited 5d shell. This results in excited states with two configurations as follows: a high-spin ^9D_J state and a ^7D_J low-spin state.[65] According to Hund's rule, the ^9D_J states have a lower energy than the ^7D_J states. However, the $^7F_J \rightarrow ^7D_J$ transitions are spin-allowed and connected with the excitation band of the transition, which has a maximum at approximately 235 nm.[66,67] Normally, the spin-forbidden $^7F_J \rightarrow ^9D_J$ transitions can be observed in the range of 250–280 nm, and all of the studied samples exhibited very weak intensities.
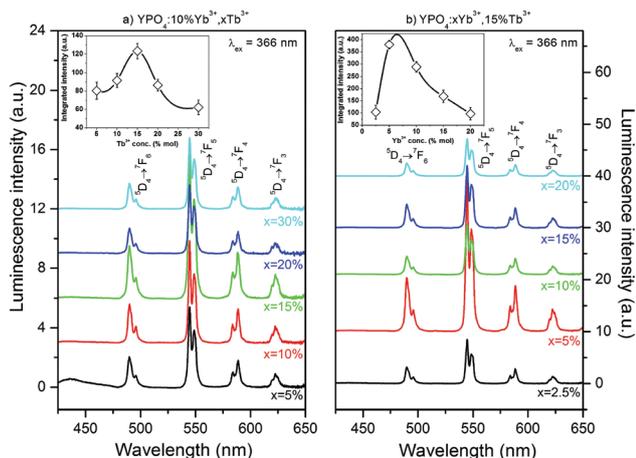
Fig. 5 Emission spectra of (a) YPO$_4$ doped with 10% Yb^{3+}, x% Tb^{3+} and (b) YPO$_4$ doped with x% Yb^{3+}, 15% Tb^{3+}; dependence on Tb^{3+} (a) and Yb^{3+} (b) concentrations and dependence of integral luminescence intensity on the Tb^{3+} (a) and Yb^{3+} (b) concentrations (shown in insets).

Fig. 6 Dependence of the up-conversion luminescence spectra of YPO$_4$:Yb^{3+},Tb^{3+} nanocrystals on the concentrations of Tb^{3+} (a) and Yb^{3+} (b); insets: dependence of integral intensity on the concentrations of Tb^{3+} (a) and Yb^{3+} (b) and emission in the 400–475 nm range.

The intensity of the $4f^8 \rightarrow 4f^7 5d^1$ transition band is sensitive to the concentration of the Yb^{3+} ions, as shown in Fig. 4b.

An increase in the amount of Yb^{3+} ions lowers the probability of the excitation of Tb^{3+} into the $4f^7 5d^1$ state and reduces the intensity of the excitation band associated with this process. A combination of ions, such as Tb^{3+}, has a tendency to be oxidized by the Yb^{3+} ion, which can be easily reduced to generate charge transfer states (CTSs). Indeed, in the Yb^{3+} and Tb^{3+} co-doped materials, the Tb$^{3+} \rightarrow$Yb^{3+} charge transfer has been observed.[33,68] After absorption of UV photons, energy from the Tb^{3+} ions that was excited into the $4f^7 5d^1$ state is transferred to the Yb^{3+} ions *via* emission at NIR wavelengths.

This process requires the existence of an intermediate Tb^{4+}–Yb^{2+} CTS.[68] The Tb^{4+}–Yb^{2+} CTS has an energy higher than the $4f^7 5d^1$ state of the Tb^{3+} ions, but thermally induced crossing between states is possible. In addition, the Tb$^{3+} \rightarrow$Yb^{3+} energy transfer to the CTS is 10–10^2 times faster than the relaxation of Tb^{3+} from the $4f^7 5d^1$ state to the $^5D_4$ excited state. Therefore, this charge transfer based mechanism explains the observed changes in the excitation spectra and quenching of the $4f^8 \rightarrow 4f^7 5d^1$ excitation band.

Fig. 5 and 6 show the luminescence spectra which were measured using UV (366 nm) or NIR (980 nm) excitation, of the Yb^{3+} and Tb^{3+} co-doped YPO$_4$ nanocrystals. The spectra in Fig. 5 exhibit characteristic luminescence bands associated with the f–f electronic transitions of Tb^{3+} ions. These transitions are due to radiative relaxation from the Tb^{3+} $^5D_4$ energy level to the ^7F_J components of the ground state. Emission from higher levels (*i.e.*, $^5G_6$ and $^5D_3$) was not observed in the samples due to cross-relaxation processes (CR) associated with the Tb^{3+} ions.[69,70] This process depopulated the $^5D_3$ state of the Tb^{3+} ion and transferred the energy difference between the $^5D_3$ and $^5D_4$ states to the neighbouring Tb^{3+} ion. This energy difference match the energy gap between $^7F_6$ and $^7F_0$ energy
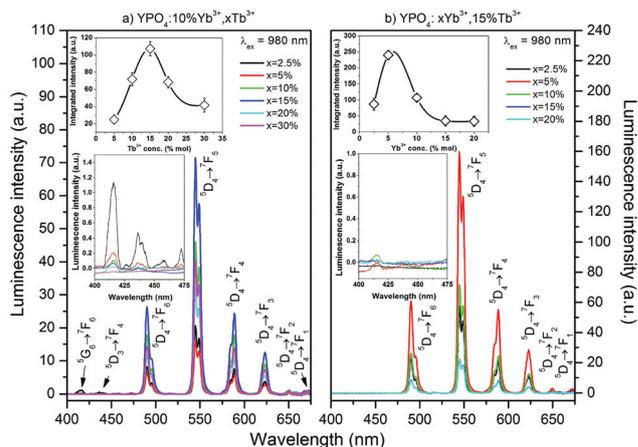
levels of the Tb^{3+} ion.[70,71] The emission peaks at 489, 544, 588 and 622 nm can be assigned to the $^5D_4 \rightarrow {}^7F_{6,5,4,3}$ transitions, respectively, and are responsible for the green luminescence under UV irradiation of the prepared materials.

The insets shown in Fig. 5 show the integral luminescence intensity of the Tb^{3+} ions as a function of the concentration of (a) Tb^{3+} or (b) Yb^{3+} ions. The sample that exhibited the most intense luminescence was doped with 5% of Yb^{3+} and 15% of Tb^{3+} ions. A concentration of Tb^{3+} ions higher than 15% caused quenching of the green luminescence. In addition, a concentration of Yb^{3+} ions higher than 5% decreased the Tb^{3+} luminescence intensity. In materials doped with Ln^{3+} ions, non-radiative processes, such as multiphonon decay, quenching by impurities or energy migration among active ions, are typically responsible for luminescence quenching. For Tb^{3+} ions, multiphonon relaxation can be neglected due to the high energy gap between the $^5D_3$ and $^5D_4$ or $^5D_4$ and ^7F_J levels, which require at least 5 or 15 phonons, respectively, to depopulate these excited states (YPO$_4$ lattice phonon energy is approximately 1080 cm^{-1}).[72] The observed emission quenching as the concentration of Tb^{3+} ions increased may be due to the energy transfer between two Tb^{3+} ions in the $^5D_4$ excited state. As the result of this process, one ion is excited into upper lying levels. However, the second ion becomes depopulated. This process can also be explained by the slight increase in the luminescence intensity of the measured emission decays (see ESI†).[73]

In fact, the observed increase in the luminescence intensity as the amount of Yb^{3+} ions increased in the sample is important. According to the literature, the Yb^{3+} ions strongly quench the emission of the Tb^{3+} ions due to cooperative energy transfer from the Tb^{3+} ion in its $^5D_4$ excited state to two Yb^{3+} ions.[49,68] This effect can be observed in the luminescence intensity when the Yb^{3+} concentration was higher than 10% or as the shortening of Tb^{3+} luminescence lifetimes in the whole range of Yb^{3+} concentrations (see Fig. 9). Similar results for

the changes in the luminescence intensity as the amount Yb^{3+} ions increased have also been previously reported.[68,74] However, the cause of this unexpected phenomenon was not explained and remains unclear. The mechanism of this anomaly may be connected to the expansion of the crystal cell volume after co-doping with Yb^{3+} ions. Cooperative energy transfer is effective only over very short distances between interacting ions.[75] Therefore, an increase in the cell volume decreases the efficiency of CET between Tb^{3+} and Yb^{3+} ions. If other processes, such as phonon assisted energy transfer (PET), quench the Tb^{3+} ions luminescence, another explanation of the observed initial increase in Tb^{3+} luminescence intensity is a backward energy transfer from neighbouring Yb^{3+} ions that also pump the $^5D_4$ excited state of the Tb^{3+} ion.

The up-conversion emission spectra of the co-doped YPO_4 thermally treated at 900 °C were observed after excitation at 980 nm, and the results are shown in Fig. 6. The spectra are similar to those obtained by UV excitation. The maximum green emission was recorded for the sample doped with 15% Tb^{3+} and 5% Yb^{3+} ions. The insets (see Fig. 6) show the integral luminescence intensity as a function of the concentration of Tb^{3+} or Yb^{3+} ions. The estimated optimal concentrations of Yb^{3+} and Tb^{3+} ions demonstrate that a relatively large portion of the Y^{3+} ions in the host material must be replaced, especially by the acceptor (i.e., Tb^{3+} ions). This fact is a direct result of the relatively low probability of CET and small distances between interacting ions, which are effective for this process.[75] In addition to the emission from the $^5D_4$ excited state, small peaks associated with the transitions from the $^5G_6$ and $^5D_3$ states were observed and are shown in the insets in Fig. 6.

The UC emission in the Yb^{3+}/Tb^{3+} system is rare, and there are only a few reports regarding up-conversion from excited states higher than $^5D_4$.[30,38,75–78] The only way to produce Tb^{3+} ions in the $^5D_3$ or $^5G_6$ excited state is via a three photon process. The Tb^{3+} ion in the populated $^5D_4$ level can be further excited up to the $^5D_1$ level by one photon through the ESA or by energy transfer from a neighbouring Yb^{3+} ion. In addition, cooperative energy transfer from three Yb^{3+} ions is possible.[78] The power dependence of the Tb^{3+} emission (see Fig. 7) confirms these assumptions. In our previous studies of Yb^{3+}/Tb^{3+} co-doped $LaPO_4$ and $GdPO_4$ hosts, we did not detect emission from the $^5D_3$ state of Tb^{3+} ions, which may be due to the different crystal system in YPO_4.[48,49]

The dependence of the integral luminescence intensity on the pumping laser power at 980 nm can provide insight into the number of photons involved in the excitation process. The relationship between the UC intensity I_{UC} and the pumping laser intensity I_P is given by the following equation:

$$I_{UC} = \alpha(I_P)^n \qquad (1)$$

where α is a proportionality factor and the exponent n represents the number of photons involved in the UC process.[29] Fig. 7 demonstrates the integral luminescence intensity as a function of the energy of the pumping laser.
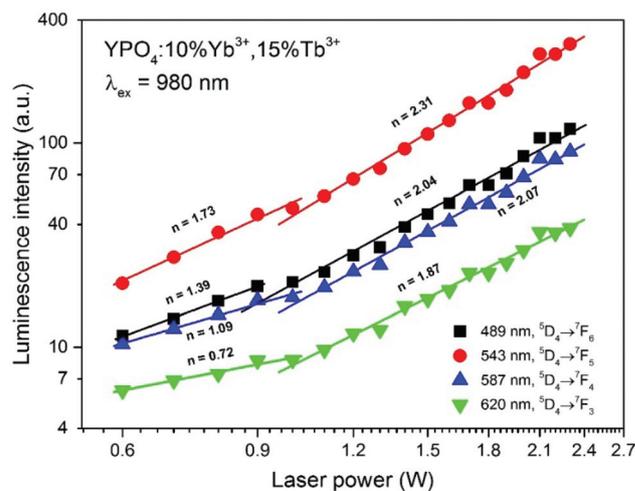

Fig. 7 Integral emission intensity of the YPO_4:10%Yb^{3+},15%Tb^{3+} sample as a function of the pumping power of the NIR laser (980 nm).

The power dependence of the luminescence intensity shown in Fig. 7 is complex. The differences between the slopes calculated for each transition of the Tb^{3+} ions indicate that the up-conversion mechanism involves additional processes, which results in divergence between the obtained values. In addition, when the power of the pumping laser was more than 1 W, the energy transfer mechanism changed, and the number of photons involved in this process was higher. According to the conditions required to match the differences between the Tb^{3+} and Yb^{3+} energy levels, cooperative energy transfer has been previously proposed in many studies.[30,31,35–37,45,79,80] The most likely process involves a simultaneous interaction of two excited Yb^{3+} ions with one Tb^{3+}, which results in excitation of the Tb^{3+} ions into a $^5D_4$ state. However, at low temperatures, GSA and ESA processes also lead to UC of Tb^{3+} ions after Yb^{3+} excitation.[35,36] The proposed scheme of the energy transfer mechanism between Yb^{3+} and Tb^{3+} ions in the YPO_4 matrix is presented in Fig. 8.
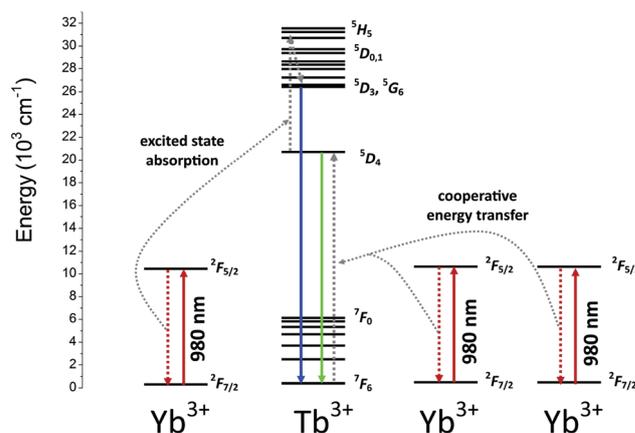

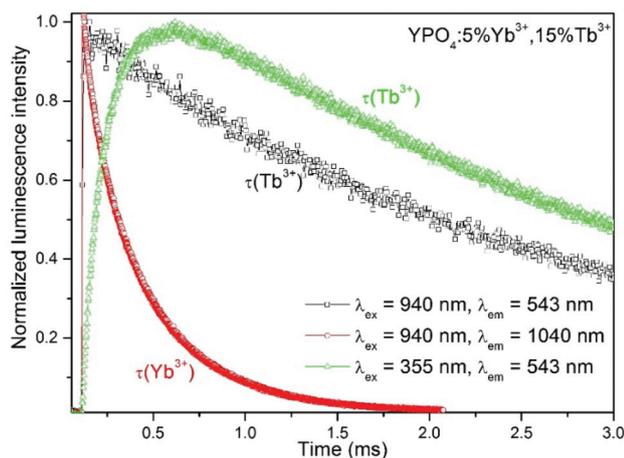**Fig. 8** The proposed scheme of energetic processes occurring in the YPO_4:Yb^{3+},Tb^{3+} samples.

Fig. 9 Luminescence decays of the YPO_4:5%Yb^{3+},15%Tb^{3+} nanocrystals.

In general, the up-conversion in the Yb^{3+} and Tb^{3+} doped YPO_4 samples can be treated as a two photon process. The observed deviations from the theoretical value can be explained as described below. The cross-relaxation (CR) that populates the $^5D_4$ state from the $^5D_3$ excited state of the Tb^{3+} ion is the most likely cause of more than 2 photons being involved in the observed UC. When the energies of the excitation source are less than 1 W, competitive processes occur and lead to quenching of the Tb^{3+} emission.

The energy transfer (ET) between the Yb^{3+} and Tb^{3+} ions is responsible for the relatively large increase in time observed in the luminescence decay of Tb^{3+} ions after excitation at 940 nm (see Fig. 9). A comparison of the luminescence decay of Yb^{3+} and Tb^{3+} after excitation at 940 nm indicated ET processes. During the time when emission from the Yb^{3+} ions disappeared, an increase in the luminescence of Tb^{3+} ions, which are the energy acceptors, was observed.

The luminescence decays of the Tb^{3+} and Yb^{3+} ions in all of the samples measured using UV and NIR laser light (355 nm and 940 nm) are reported in the ESI.† The recorded decays were used to calculate luminescence lifetimes, which are compared in Fig. 10. The shapes of the measured Tb^{3+} and Yb^{3+} luminescence decay curves (λ_{ex} = 355 nm or 940 nm) were non-exponential due to the quenching processes. However, the decrease in the lifetime may still be approximated using an exponential function. The single exponential model for the lifetime value calculations of the Tb^{3+} and Yb^{3+} ion (Fig. 10a, b, d and e) luminescence was as follows:

$$I = I_0 e^{-\frac{t}{\tau}} \qquad (2)$$

where I represents the intensity at any time, I_0 is the intensity at $t = 0$ and τ is the luminescence lifetime.

Luminescence decays of Tb^{3+} ions, which result from up-conversion (λ_{ex} = 940 nm), exhibited rise times in all of the samples. Therefore, to calculate the luminescence lifetimes and rise times, the following equation was used:
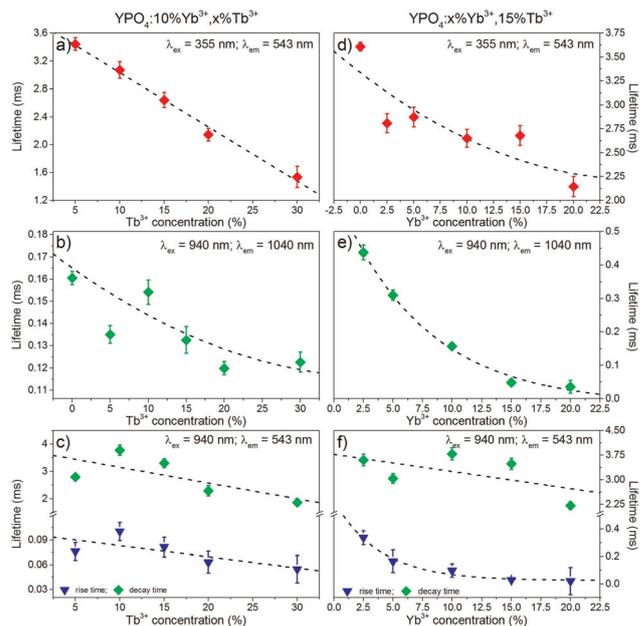

Fig. 10 Luminescence lifetimes of the Tb^{3+} (a, c, d, f) and Yb^{3+} (b, e) ions in the YPO_4 nanocrystals, which are as dependent on the concentration of Tb^{3+} (a, b, c) or Yb^{3+} (d, e, f).

$$I = [I_0 + I_1(1 - e^{-\frac{t}{\tau_r}})]e^{-\frac{t}{\tau_d}} \qquad (3)$$

where I_0 is the initial luminescence intensity at time $t = 0$, I_1 is the intensity added by the energy transfer, and τ_r and τ_d are the rise and decay times, respectively. This equation fits the decay profiles well for all of the samples. The calculated luminescence lifetimes and rise times are compared in Fig. 10.

The decay times were dependent on the dopant concentration and became shorter with increasing amounts of Tb^{3+} or Yb^{3+} ions in the YPO_4 host for each excitation wavelength used. In more highly doped samples, the distance between the donor and acceptor ions is shorter, and therefore, the energy transfer occurs faster. In addition, phenomena such as cross-relaxation and cooperative energy transfer become more effective. The calculated values of the luminescence lifetimes of the Tb^{3+} ions are typical for this ion for UV (355 nm) and NIR (940 nm) excitations and are in the range of 1.5–3.8 ms. The use of UV light for excitation caused much more effective quenching as the amounts of Tb^{3+} or Yb^{3+} ions increased compared to NIR radiation, and this result was especially noticeable in samples doped with 30% Tb^{3+} ions (Fig. 10a, c, d and f). The highly energetic UV photons generate larger numbers of quenching centres than those generated from NIR radiation. In addition, the lifetimes of Yb^{3+} were typical for this ion and are in the range of 0.12–0.48 ms. The effect of the increasing Tb^{3+} ion concentration on the luminescence lifetimes of the Yb^{3+} ions (Fig. 10b) is in agreement with the proposed energy transfer from Yb^{3+} to Tb^{3+} ions. The shortened lifetimes associated with an increased amount of Tb^{3+} ions confirm the effectiveness of this process. However, the relatively simple electronic structure of the Yb^{3+} ions is not conducive

for concentration quenching, and this effect is visible in Fig. 10b where a shortening in the Yb^{3+} lifetimes occurs when the concentration of this ion was increased due to the presence of Yb^{2+} ions or by radiation trapping caused by the presence of resonant $^2F_{7/2} \leftrightarrow {}^2F_{5/2}$ transitions between Yb^{3+} ions.[81]

The calculated values of the rise times of Tb^{3+} luminescence (Fig. 10c and f) are comparable to the lifetimes of Yb^{3+} ions when we take into account the proposed CET up-conversion mechanism. The longest rise times were calculated for samples doped with 10% Tb^{3+} ions in the series of samples shown in Fig. 10c or 2.5% Yb^{3+}, which is shown in Fig. 10f.

The efficiency of the cooperative energy transfer between the Yb^{3+} and Tb^{3+} ions can be estimated based on the measured luminescence decays. The method of calculation has been previously described.[31] In short, the following equation can be used to calculate the cooperative energy transfer efficiency (η_{CET}) for different Tb^{3+} ion concentrations:

$$\eta_{CET} = 1 - \frac{\tau_{Yb-Tb}}{\tau_{Yb}} \qquad (4)$$

where τ_{Yb-Tb} is the lifetime of Yb^{3+} ions in the presence of Tb^{3+} and τ_{Yb} is the lifetime of Yb^{3+} in the absence of Tb^{3+} ions. This method is also useful for the estimation of a backward energy transfer efficiency (η_{BT}), which can be expressed as

$$\eta_{BT} = 1 - \frac{\tau_{Tb-Yb}}{\tau_{Tb}} \qquad (5)$$

where τ_{Tb-Yb} is the lifetime of Tb^{3+} ions in the presence of Yb^{3+} and τ_{Tb} is the lifetime of Tb^{3+} in the absence of Yb^{3+} ions.

The calculated values of both parameters (*i.e.*, η_{CET} and η_{BT}) are plotted in Fig. 11. The energy transfer efficiency increased as the amount of Tb^{3+} ions in the YPO_4 host increased. Therefore the highest up-conversion was observed for the largest concentrations used. However, the backward energy transfers are also very effec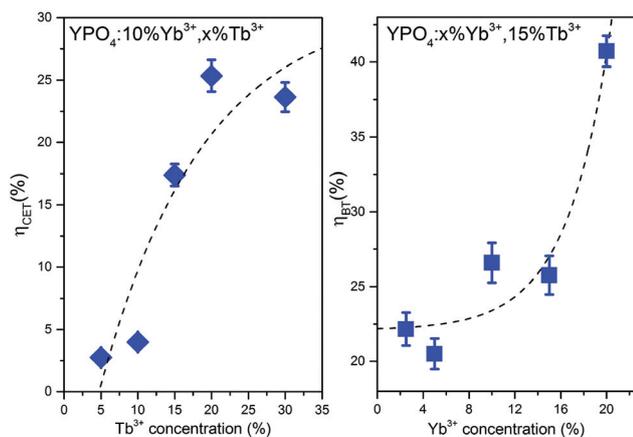tive in the studied system and become high when Yb^{3+} concentrations exceed 10%. Therefore, these materials can also be promising down-conversion systems.

Conclusions

Rare earth co-doped YPO_4 nanocrystals can be synthesized using a co-precipitation method. To obtain efficient UV-excited and up-conversion luminescence, annealing of the as-prepared tetragonal nanocrystals at 900 °C is necessary. As a result of the thermal treatment, the obtained materials consisting of nanofibers were converted to spherical nanocrystals. The XRD studies confirmed that the obtained materials were a single phase with a tetragonal crystal structure in the $I4_1/amd$ space group.

The observed luminescence exhibited a dual mode nature. The prepared materials could be excited by UV or NIR radiation yielding intense green luminescence. The spectroscopic properties were analysed using both UV and NIR wavelengths as excitation sources. The excitation spectra indicated the presence of a charge transfer $Tb^{4+} \rightarrow Yb^{2+}$ state in the samples. The best dopant concentrations that resulted in the highest luminescence upon UV light (365 nm) or NIR (980 nm) excitation were 5% Yb^{3+} ions and 15% Tb^{3+} ions. In addition to the typical Tb^{3+} ion emission from the $^5D_4$ excited state, emission bands associated with the transitions from the $^5G_6$ and $^5D_3$ states were observed due to up-conversion. The effects of the presence of other quenching processes, such as cross-relaxation between Tb^{3+} ions, multiphonon quenching and backward energy transfer from Yb^{3+} to Tb^{3+} ions were determined. The dependence of the integral up-conversion luminescence intensity on the pumping laser power confirmed that at least two photons participated in the excitation of the Tb^{3+} ions. In addition, evidence of a three photon process was observed (*i.e.*, increasing slope of the curves above 2). The recorded emission decays exhibited a relatively long rise in the luminescence intensity after the laser pulse, which confirmed that an energy transfer occurred between the Yb^{3+} and Tb^{3+} ions. The obtained results present a route for the synthesis of YPO_4 nanocrystals doped with Yb^{3+} and Tb^{3+} ions showing efficient UV-excited luminescence, as well as up-conversion under NIR radiation.

Acknowledgements

Fig. 11 Cooperative energy transfer efficiency (η_{CET}) and backward energy transfer efficiency (η_{BT}) as functions of the Tb^{3+} or Yb^{3+} concentrations.

References

1 M. Haase and H. Schäfer, *Angew. Chem., Int. Ed.*, 2011, **50**, 5808–5829.

2 D. Vennerberg and Z. Lin, *Sci. Adv. Mater.*, 2011, **3**, 26–40.

3 T. Grzyb, M. Runowski, A. Szczeszak and S. Lis, *J. Phys. Chem. C*, 2012, **116**, 17188–17196.

4 T. Grzyb, A. Szczeszak, J. Rozowska, J. Legendziewicz and S. Lis, *J. Phys. Chem. C*, 2012, **116**, 3219–3226.

5 R. Pazik, R. Tekoriute, S. Håkansson, R. Wiglusz, W. Strek, G. a Seisenbaeva, Y. K. Gun'ko and V. G. Kessler, *Chemistry*, 2009, **15**, 6820–6826.

6 M. a. M. Lucena, G. F. de Sá, M. O. Rodrigues, S. Alves, M. Talhavini and I. T. Weber, *Anal. Methods*, 2013, **5**, 705.

7 K. Pavani, J. S. Kumar, T. Sasikala, B. C. Jamalaiah, H. J. Seo and L. R. Moorthy, *Mater. Chem. Phys.*, 2011, **129**, 292–295.

8 C. C. Lin and R.-S. Liu, *J. Phys. Chem. Lett.*, 2011, **2**, 1268–1277.

9 V. Bedekar, D. P. D. Dutta, M. Mohapatra, S. V. Godbole, R. Ghildiyal and A. K. Tyagi, *Nanotechnology*, 2009, **125707**, 125707–125714.

10 S. Wang, J. Feng, S. Song and H. Zhang, *CrystEngComm*, 2013, **15**, 7142.

11 Y. Il Park, H. M. Kim, J. H. Kim, K. C. Moon, B. Yoo, K. T. Lee, N. Lee, Y. Choi, W. Park, D. Ling, K. Na, W. K. Moon, S. H. Choi, H. S. Park, S.-Y. Yoon, Y. D. Suh, S. H. Lee and T. Hyeon, *Adv. Mater.*, 2012, **24**, 5755–5761.

12 D. Tu, Y. Liu, H. Zhu and X. Chen, *Chem. – Eur. J.*, 2013, **19**, 5516–5527.

13 G. Chen, H. Qiu, P. N. Prasad and X. Chen, *Chem. Rev.*, 2014, **114**, 5161–5214.

14 L.-D. Sun, Y.-F. Wang and C.-H. Yan, *Acc. Chem. Res.*, 2014, **47**, 1001–1009.

15 W. G. van Sark, J. de Wild, J. K. Rath, A. Meijerink and R. E. Schropp, *Nanoscale Res. Lett.*, 2013, **8**, 81.

16 B. M. van der Ende, L. Aarts and A. Meijerink, *Phys. Chem. Chem. Phys.*, 2009, **11**, 11081–11095.

17 C. Brecher, *J. Chem. Phys.*, 1968, **49**, 3303.

18 S. Erdei, F. W. Ainger, D. Ravichandran, W. B. White and L. E. Cross, *Mater. Lett.*, 1997, **30**, 389–393.

19 C.-H. Yan, Z.-G. Yan, Y.-P. Du, J. Shen, C. Zhang and W. Feng, in *Handbook on the Physics and Chemistry of Rare Earths*, ed. K. A. Gschneider, J.-C. G. Bünzli and V. K. Percharsky, Elsevier, 2011, vol. 41, pp. 275–472.

20 S. Heer, O. Lehmann, M. Haase and H.-U. H.-U. Güdel, *Angew. Chem., Int. Ed.*, 2003, **42**, 3179–3182.

21 A. N. M. Yunxiang Ni and John M. Hughes, *Am. Mineral.*, 1995, **80**, 21–26.

22 N. Bloembergen, *Phys. Rev. Lett.*, 1959, **2**, 84–85.

23 F. Auzel, *C. R. Acad. Sci. Paris B*, 1966, **263**, 819–821.

24 F. Auzel, *C. R. Acad. Sci. Paris B*, 1966, **262**, 1016–1019.

25 F. Auzel, *Chem. Rev.*, 2004, **104**, 139–173.

26 W. Feng, C. Han and F. Li, *Adv. Mater.*, 2013, 1–17.

27 A. Gnach and A. Bednarkiewicz, *Nano Today*, 2012, **7**, 532–563.

28 M. Lin, Y. Zhao, S. Wang, M. Liu, Z. Duan, Y. Chen, F. Li, F. Xu and T. Lu, *Biotechnol. Adv.*, 2012, **30**, 1551–1561.

29 R. Scheps, *Prog. Quantum Electron.*, 1996, **20**, 271–358.

30 L. de S. Menezes, G. S. Maciel, C. B. de Araújo and Y. Messaddeq, *J. Appl. Phys.*, 2003, **94**, 863.

31 Y. Arai, T. Yamashidta, T. Suzuki and Y. Ohishi, *J. Appl. Phys.*, 2009, **105**, 83105–83111.

32 B. Lai, J. Wang and Q. Su, *Appl. Phys. B*, 2009, **98**, 41–47.

33 X. Liu, S. Ye, Y. Qiao, G. Dong, B. Zhu, D. Chen, G. Lakshminarayana and J. Qiu, *Appl. Phys. B*, 2009, **96**, 51–55.

34 M. a. Noginov, P. Venkateswarlu and M. Mahdi, *J. Opt. Soc. Am. B*, 1996, **13**, 735.

35 G. Salley, R. Valiente and H. Güdel, *Phys. Rev. B: Condens. Matter*, 2003, **67**, 1–9.

36 G. M. Salley, R. Valiente and H. U. Guedel, *J. Lumin.*, 2001, **94–95**, 305–309.

37 V. Scarnera, B. Richards, A. Jha, G. Jose and C. Stacey, *Opt. Mater.*, 2010, **33**, 159–163.

38 C. H. Yang, Y. X. Pan, Q. Y. Zhang and Z. H. Jiang, *J. Fluoresc.*, 2007, **17**, 500–504.

39 Z. Yang, D. Yan, Z. Song, D. Zhou, X. Yu, Y. Yang, Z. Yin, L. Yan, R. Wang, H. Wu and J. Qiu, *J. Lumin.*, 2012, **132**, 1550–1552.

40 K. Zhu, Z. Yang, D. Yan, Z. Song, D. Zhou, R. Wang and J. Qiu, *J. Sol-Gel Sci. Technol.*, 2012, **62**, 149–152.

41 K. Prorok, A. Gnach, A. Bednarkiewicz and W. Stręk, *J. Lumin.*, 2013, **140**, 103–109.

42 P. Vergeer, T. Vlugt, M. Kox, M. den Hertog, J. van der Eerden and A. Meijerink, *Phys. Rev. B: Condens. Matter*, 2005, **71**, 1–11.

43 L. Li, X. Wei, Y. Chen, C. Guo and M. Yin, *J. Rare Earths*, 2012, **30**, 197–201.

44 Y.-T. An, C. Labbé, J. Cardin, M. Morales and F. Gourbilleau, *Adv. Opt. Mater.*, 2013, **1**, 855–862.

45 M. L. Debasu, D. Ananias, S. L. C. Pinho, C. F. G. C. Geraldes, L. D. Carlos and J. Rocha, *Nanoscale*, 2012, **4**, 5154–5162.

46 W. Ren, G. Tian, L. Zhou, W. Yin, L. Yan, S. Jin, Y. Zu, S. Li, Z. Gu and Y. Zhao, *Nanoscale*, 2012, **4**, 3754–3760.

47 M. L. Debasu, D. Ananias, J. Rocha, O. L. Malta and L. D. Carlos, *Phys. Chem. Chem. Phys.*, 2013, **15**, 15565–15571.

48 T. Grzyb, A. Gruszeczka, R. J. Wiglusz, Z. Śniadecki, B. Idzikowski and S. Lis, *J. Mater. Chem.*, 2012, **22**, 22989–22997.

49 T. Grzyb, A. Gruszeczka, R. J. Wiglusz and S. Lis, *J. Mater. Chem. C*, 2013, **1**, 5410–5418.

50 D. Bish and J. Post, *Am. Mineral.*, 1993, **78**, 932–940.

51 H. M. Rietveld, *J. Appl. Crystallogr.*, 1969, **2**, 65–71.

52 A. Hezel and S. D. Ross, *J. Inorg. Nucl. Chem.*, 1967, **29**, 2085–2089.

53 G. M. Begun, G. W. Beall, L. A. Boatner and W. J. Gregor, *J. Raman Spectrosc.*, 1981, **11**, 273–278.

54 D. F. Mullica, D. A. Grossie and L. A. Boatner, *Inorg. Chim. Acta*, 1985, **109**, 105–110.

55 H. Meyssamy, K. Riwotzki, A. Kornowski, S. Naused and M. Haase, *Adv. Mater.*, 1999, **11**, 840–844.

56 K. Riwotzki, H. Meyssamy, A. Kornowski and M. Haase, *J. Phys. Chem. B*, 2000, **104**, 2824–2828.

57 N. K. Sahu, R. S. Ningthoujam and D. Bahadur, *J. Appl. Phys.*, 2012, **112**, 014306.

58 J. Cybińska, C. Lorbeer and A.-V. Mudring, *J. Mater. Chem.*, 2012, **22**, 9505.

59 T. Shimizu and T. Isobe, *IOP Conf. Ser. Mater. Sci. Eng.*, 2011, **18**, 032021.

60 J. Wang, Y. Xu, M. Hojamberdiev, Y. Cui, H. Liu and G. Zhu, *J. Alloys Compd.*, 2009, **479**, 772–776.

61 P. P. Fedorov, M. N. Mayakova, S. V. Kuznetsov, V. V. Voronov, R. P. Ermakov, K. S. Samarina, A. I. Popov and V. V. Osiko, *Mater. Res. Bull.*, 2012, **47**, 1794–1799.

62 P. P. Fedorov, A. a. Luginina, S. V. Kuznetsov and V. V. Osiko, *J. Fluorine Chem.*, 2011, **132**, 1012–1039.

63 R. J. Wiglusz, R. Pazik, A. Lukowiak and W. Strek, *Inorg. Chem.*, 2011, 300–301.

64 P. Ayyub, V. Palkar, S. Chattopadhyay and M. Multani, *Phys. Rev. B: Condens. Matter*, 1995, **51**, 6135–6138.

65 L. Ning, C. Mak and P. Tanner, *Phys. Rev. B: Condens. Matter*, 2005, **72**, 085127.

66 L. Yang, L. Zhou, X. Chen, X. Liu, P. Hua, Y. Shi, X. Yue, Z. Tang and Y. Huang, *J. Alloys Compd.*, 2010, **509**, 3866–3871.

67 R. J. Wiglusz and T. Grzyb, *Opt. Mater.*, 2011, **33**, 1506–1513.

68 J.-L. Yuan, X.-Y. Zeng, J.-T. Zhao, Z.-J. Zhang, H.-H. Chen and X.-X. Yang, *J. Phys. D: Appl. Phys.*, 2008, **41**, 105406.

69 P. C. Ricci, M. Salis, R. Corpino, C. M. Carbonaro, E. Fortin and A. Anedda, *J. Appl. Phys.*, 2010, **108**, 43512–43517.

70 A. D. Sontakke, K. Biswas and K. Annapurna, *J. Lumin.*, 2009, **129**, 1347–1355.

71 P. Berdowski, M. J. J. Lammers and G. Blasse, *Chem. Phys. Lett.*, 1985, **113**, 387–390.

72 A. K. Parchur, A. I. Prasad, S. B. Rai, R. Tewari, R. K. Sahu, G. S. Okram, R. A. Singh and R. S. Ningthoujam, *AIP Adv.*, 2012, **2**, 032119.

73 T. Grzyb and S. Lis, *Inorg. Chem.*, 2011, **50**, 8112–8120.

74 X. Y. Huang, D. C. Yu and Q. Y. Zhang, *J. Appl. Phys.*, 2009, **106**, 113521.

75 T. Yamashita and Y. Ohishi, *J. Non-Cryst. Solids*, 2008, **354**, 1883–1890.

76 R. Martín-Rodríguez, R. Valiente, S. Polizzi, M. Bettinelli, A. Speghini and F. Piccinelli, *J. Phys. Chem. C*, 2009, **113**, 12195–12200.

77 J. Adam, N. Duhamel-Henry and J. Allain, *J. Non-Cryst. Solids*, 1997, **213–214**, 245–250.

78 L. Huang, T. Yamashita, R. Jose, Y. Arai, T. Suzuki and Y. Ohishi, *Appl. Phys. Lett.*, 2007, **90**, 131116–131119.

79 I. a. a. Terra, L. J. Borrero-González, L. a. O. Nunes, M. P. Belançon, J. H. Rohling, M. L. Baesso and O. L. Malta, *J. Appl. Phys.*, 2011, **110**, 083108.

80 W. Stręk, A. Bednarkiewicz and P. J. Dereń, *J. Lumin.*, 2001, **92**, 229–235.

81 G. Boulon, *J. Alloys Compd.*, 2008, **451**, 1–11.